Enhanced ion acoustic fluctuations in laser-produced plasmas

W. Rozmus and V. T. Tikhonchuk*
Department of Physics, University of Alberta, Edmonton, Alberta, Canada T6G 2J1

V. Yu. Bychenkov
P. N. Lebedev Physics Institute, Russian Academy of Sciences, Moscow 117924, Russia

C. E. Capjack
Department of Electrical Engineering, University of Alberta, Edmonton, Alberta, Canada T6G 2G7
(Received 30 March 1994; revised manuscript received 14 July 1994)

The nonuniform laser heating of a plasma has been identified as contributing to a source of enhanced ion acoustic fluctuations that occur during the initial phase of the laser plasma interaction process. The resulting temperature gradient creates a heat flux that is responsible for the excitation of unstable ion waves, which propagate predominantly in a plane perpendicular to the laser beam axis. We have used the results of weak turbulence theory to estimate the stationary level and the angular distribution of these fluctuations. These are shown to have a dramatic effect on the Brillouin scattering reflectivity. The importance of this ion wave enhancement mechanism for the short (10 ps) laser pulse interaction experiments is discussed.

PACS number(s): 52.35.Qz, 52.35.Ra, 52.40.Nk

I. INTRODUCTION

One of the main challenges in laser-driven inertial confinement fusion (ICF) research [1,2] is the stimulated scattering of laser radiation in the plasma corona. In spite of almost two decades of intense experimental and theoretical studies, we can neither control these instabilities nor reliably predict reflectivities from large scale plasmas that are characteristic of future reactor experiments. One of the difficulties encountered in the theoretical description of laser light scattering is related to the complexity of ICF targets. The presence of a strong driver will remove the plasma from the thermal equilibrium state by altering the particle distribution function, and will also impose spatial gradients in both the plasma density and temperature. In addition, various scattering processes such as stimulated Raman scattering (SRS), stimulated Brillouin scattering (SBS), and filamentation or self-focusing instabilities can occur simultaneously. The complicated nonlinear coupling between these processes can significantly alter noise levels and local values of hydrodynamic and laser beam parameters. This makes the quantitative prediction of laser scattering levels an extremely difficult task.

Recently, new experiments with well characterized preformed plasmas and picosecond laser pulse durations [3] have helped to simplify the study of the physics of scattering instabilities. The use of relatively short interaction times results in minimal hydrodynamic plasma evolution. This allows a theoretical analysis which is based on the standard linearized wave coupling equations to be used. However, the quantitative comparison between measured reflectivities [3] and theoretical calculations [4] still show large discrepancies. The most likely source of this difference is the low level of the initial thermal equilibrium fluctuations that is used in the theoretical model.

The source of the initial electrostatic fluctuations in a plasma (cf. Refs. [4–6]) for the scattering instabilities is usually attributed to discrete particle effects. However, in order to quantitatively interpret SBS measurements in laser interaction experiments with preformed plasmas [3,7], one must use enhanced ion acoustic fluctuation levels. Several different processes may be responsible for these fluctuations. Instabilities at the quarter critical density $n_c/4$ such as two plasmon decay have been identified as a seeding mechanism for ion acoustic fluctuations and SBS in the experiment by Young *et al.* [7]. A theoretical scenario in which the nonlinear evolution of Langmuir waves produced by SRS drives a high level of ion acoustic waves (IAW's) and hence enhanced Brillouin reflectivity has been advanced by Kolber *et al.* [8]. In this mechanism, SRS is saturated through the coupling of Langmuir waves and ion fluctuations. Another SBS enhancement mechanism in laser-produced plasmas is proposed in Ref. [9]. This is related to the heat flux driven ion acoustic instability discovered by Forslund [10]. De Groot *et al.* [11] recently suggested that part of the backscattered light in thin foil experiments [12] (the blueshifted component) can be attributed to Brillouin scattering off ion fluctuations produced by heat flux driven instabilites. In this paper we examine this mechanism in greater detail by investigating a specific interaction geometry. Quantitative estimates of the density fluctuation level and the laser light scattering efficiency will be developed.

*On leave from P. N. Lebedev Physics Institute, Russian Academy of Sciences, Moscow 117924, Russia.

We discuss the ion acoustic wave instability that is driven by the electron heat flux that results from the initial, nonuniform inverse bremsstrahlung heating of a plasma. The focused laser beam creates and maintains a temperature gradient normal to the direction of laser propagation, particularly during the first several tens of ps when the ions do not have sufficient time to move. These are typical conditions in the interaction of lasers with preformed plasmas. This heat flux driven instability is also important in plasmas created by laser pulses with random phase plate (RPP) optics or with induced spatial incoherence (ISI), where many Gaussian-like hot spots are produced in an attempt to smooth out and control laser intensity nonuniformities. By taking the thermal flux driven instability [10] as the starting point, we describe the characteristic levels and angular distribution of the ion acoustic fluctuations that are produced after the saturation of the linear instability. Our discussion is based upon the results of weak ion acoustic turbulence theory [13,14] which will be used to develop an estimate of the level of Brillouin scattering that is expected from ion fluctuations produced by heat flux driven instabilities.

Our paper is organized as follows. Section II describes threshold conditions for the heat flux driven IAW instability in the presence of temperature gradients created by a Gaussian laser pulse interacting with a homogeneous plasma. It also contains results of the numerical simulations of the laser plasma heating. Section III applies the results of weak turbulence theory to laser heated plasmas. Sec. IV gives predictions for the Brillouin reflectivity from enhanced ion fluctuations and relates these to experimental observations. Finally Sec. V contains a summary and short discussion of ion fluctuations produced by RPP laser pumps and of their role in different parametric instabilities such as stimulated Raman scattering.

II. HEAT FLUX DRIVEN ION ACOUSTIC INSTABILITY IN LASER-PRODUCED PLASMAS

The inverse bremsstrahlung absorption of a laser pulse with a Gaussian-like radial profile by a plasma results in strong temperature gradients in the direction perpendicular to the laser beam axis. At first, the particle density is only weakly disturbed and the plasma response is dominated by a heat front propagating across the plasma toward the outer edges of the laser beam. This is a transient effect, and the strong temperature gradient may later disappear due to plasma convection. However, it can dominate the entire plasma evolution during short pulse ($\approx$ 10 ps) interaction experiments [3]. The energy transported down the temperature gradient is carried by fast electrons. As a result of this heat flux, an electric field is generated which will drive a return current of electrons from the bulk of the distribution function. When this return current is above a threshold value, it gives rise to kinetic [10] or hydrodynamic [15,16] ion acoustic instabilities.

The threshold condition for the heat flux driven ion acoustic instability can be written in terms of the incident laser light intensity I_0 and the threshold value of the electron heat flux $n_e c_s T_e$ (cf. [16]) as

$$I_0 \gtrsim n_e T_e c_s / A, \tag{1}$$

where n_e and T_e are the electron density and temperature, c_s is the ion acoustic velocity, and A is the laser energy absorption coefficient. Equation (1) is easily satisfied in most experiments, however, the threshold condition is oversimplified. Therefore a more detailed analysis of the evolution of the temperature distribution during interaction of a laser pulse with a preformed plasma is necessary. We will develop a simple transport model of plasma heating by a Gaussian pulse and benchmark this against more complete hydrodynamic simulations. The simplified model will be used in the theoretical analysis that follows.

A. Stationary model of the plasma heating

Let us first assume that the plasma density is homogeneous and that it does not change during the time of the interaction. Due to the absorption of the laser beam energy, the plasma will be heated preferentially in the central region of the beam and will remain cooler toward the laser beam edges because of thermal conduction losses. We can find the electron temperature distribution from the heat transport equation

$$\frac{3}{2} n_e \frac{\partial T_e}{\partial t} + \vec{\nabla} \cdot \vec{q} = \frac{\nu_{ei} n_e}{c n_c} I_0(\vec{r}, t), \tag{2}$$

where n_c is the critical electron density, ν_{ei} is the electron-ion collision frequency, and $\vec{q}$ is the electron heat flux. In our analytical model we assume the heat flux to be classical, $\vec{q} = -\zeta(Z) n_e v_{Te}^2 \nu_{ei}^{-1} \vec{\nabla} T_e$ where the ion charge dependent coefficient $\zeta = 4.42(Z + 1.7Z^2)/(0.8 + 2.4Z + 0.6Z^2)$ is taken from Ref. [16] and $v_{Te} = \sqrt{T_e/m_e}$ is the electron thermal velocity. The classical heat conductivity in Eq. (2) limits applicability of the model to relatively small temperature gradients in the plasma. The importance of this limitation will be examined through a comparison with results of hydrodynamical simulations. By investigating the effects of thermal transport over a wide parameter range, from strongly inhibited to free streaming limits, we find that the classical heat flux gives reasonable results for the case of short wavelength lasers. In all cases, the heat flux predicted by the hydrodynamic code remains above the threshold (1) for the return current instability. However, for cases of long wavelength lasers our simple model (2) underestimates temperature and overestimates heat fluxes in a more significant way.

An estimate of the characteristic plasma heating time τ_H can be found by comparing the inverse bremsstrahlung heating rate [right hand side of Eq. (2)] with the time derivative of T_e under the assumption of no heat flux losses,

$$\tau_H \approx n_c T_{e0} c / I_0 \nu_{ei}. \tag{3}$$

This is a short time period, typically a few picoseconds in experiments and is usually much less than the characteristic growth time of scattering instabilities and the laser pulse duration ($\tau_0 = 10$ ps in experiment [3]). A first approximation for the temperature profile across the laser beam can be obtained by solving the stationary version of Eq. (2). For the case of an axially symmetric Gaussian laser beam $I_0(r) = I_0 \exp(-r^2/a^2)$, the electron temperature distribution $T_e(r) = T_0\Theta(r/a)$ satisfies the following equation:

$$\Theta^{-3/2}\exp(-\rho^2) = -\frac{1}{\rho}\frac{d}{d\rho}\left(\rho\Theta^{5/2}\frac{d\Theta}{d\rho}\right), \qquad (4)$$

where $\rho = r/a$ is the normalized radial distance. The characteristic temperature T_0 is defined by setting the absorbed laser energy $I_0(n_e/n_c)[\nu_{ei}(T_0)a/c]$ [cf. Eq. (2)] equal to the heat flux $q_0 = \zeta n_e T_0 v_{Te}^2/a\nu_{ei}(T_0)$. This can be written as

$$T_0 = 0.2P_0^{1/5}\lambda_0^{-2/5}\left[\frac{Z^2}{\zeta(Z)}\right]^{1/5}\left(\frac{n_e}{n_c}\right)^{2/5}\Lambda^{2/5} \quad \text{keV}, \qquad (5)$$

where the laser wavelength λ_0 is given in micrometers, the total laser power $P_0 = \pi I_0 a^2$ is in gigawatts, and Λ is the Coulomb logarithm.

The numerical solution of Eq. (4) is shown in Fig. 1. The temperature starts from a maximum value $\Theta(0) \cong 0.9$ and decreases monotonically toward the edges. The on axis temperature $\Theta(0)$ can vary depending upon the choice of the background plasma temperature $\Theta(r = \infty)$. The minimum value $\Theta(0) = 0.899$ is obtained if $\Theta(r = \infty) = 0$. The profile shown in Fig. 1 corresponds to $\Theta(0) = 0.905$ which was found using the condition $T_e(0) = 3T_e(\infty)$ in order to match the numerical calculations described in the second part of this section.

Equation (5) suggests that the characteristic plasma temperature depends only on the total power of the laser beam, and not on the intensity or the radial beam size. The temperature distribution along the direction of pulse propagation is predicted to be almost constant. Any variations are related to the depletion of the laser light through absorption. The strongest laser intensity inhomogeneities occur across the laser axis, resulting in a strong radial temperature gradient and a large heat flux. For example, in experiment [3], where the laser pulse energy was approximately 10 J, Eq. (5) predicts the temperature $T_0 = 0.84$ keV (for $\Lambda = 7$) which is several times larger than the estimated initial temperature of the preformed plasma.

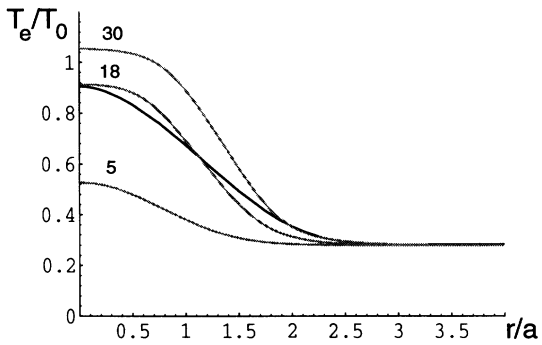

FIG. 1. The radial distribution of the electron plasma temperature obtained from the solution of Eq. (4) with the assumption $T_e(0) = 3T_e(\infty)$ (solid line). The results of the full hydrodynamic modeling using the CASTOR code are shown in gray lines for comparison. The numbers near gray lines correspond to the time moments in ps. The maximum incident laser intensity was 10^{15} W/cm^2, other parameters of the hydrodynamic simulations are $\lambda_0 = 0.335$ μm, $n_e/n_c = 0.2$, initial temperature is 300 eV.

For the case of a laser beam with a Gaussian radial profile, the solution of Eq. (4) (cf. Fig. 1) gives a heat flux $q(r) = -\Theta(d\Theta/d\rho)q_0$ which is directed radially outward. The flux is equal to zero on axis and reaches a maximum $q_{max} = 0.25q_0$ at the beam edge $r = a$, and decreases to zero outside of the laser spot. The ratio of q_{max} to the instability threshold $\frac{5}{3}n_e c_s T_e$ [16] is given by

$$\frac{q_{max}}{\frac{5}{3}n_e c_s T_e(a)} = 0.15\zeta(Z)\sqrt{\frac{m_i}{Zm_e}}\frac{\lambda_e}{a} \approx 9\zeta(Z)\frac{\lambda_e}{a}, \qquad (6)$$

where $\lambda_e = v_{Te}/\nu_{ei}$ is the electron mean free path, and can be expressed as

$$\lambda_e = 57.1\frac{1}{Z\Lambda}T_0^2\lambda_0^2\frac{n_c}{n_e} \quad \mu\text{m},$$

where T_0 has units of keV and is given by Eq. (5) and λ_0 is measured in micrometers. In experiment [3], the beam full width at half maximum (FWHM) was approximately 100 μm ($a = 60$ μm) and the electron mean free path approximately 9 μm. Hence, according to Eq. (6), the heat flux was more than six times the threshold value, for $Z = 5$.

In experiment [3], the characteristic temperature scale length a exceeds the electron mean free path by a factor of about 10. We note that for values of $a/\lambda_e \approx 50$ (cf., e.g., Ref. [17]), the electron heat flux becomes nonlocal and is considerably reduced as compared to the classical value (used in our paper). We will examine the effect of electron heat flux inhibition in the next subsection. Ion acoustic turbulence can also contribute to the thermal transport inhibition by enhancing electron collisionality. A comparison of the ion instability threshold given by Eq. (6) with the criterion for the onset of nonlocal transport effects $a/\lambda_e \lesssim 50$ suggests that in typical experimental conditions found in high Z plasmas, ion waves can become unstable approximately for the same temperature gradient scale as the reduction of the heat flux due to nonlocal effects (cf. Ref. [18]).

B. Numerical modeling of the laser plasma heating

In order to validate the simple stationary model (4) of the plasma heating and to investigate the effect of the electron heat flux inhibition on the instability threshold we compare its predictions with those of the CASTOR hy-

drodynamic simulation code [19]. We consider the example of a preformed underdense carbon plasma column that is heated by a laser beam with a Gaussian radial profile. The plasma column is assumed to be 300 μm long with initial electron and ion temperatures of 200 eV and a uniform electron density $n_e/n_c = 0.1$. A laser beam with a 1.06 μm wavelength and a FWHM vacuum focal diameter of 50 μm is focused at the center of a plasma column. The laser intensity is assumed to grow linearly from a value of 0 to the maximum value (10^{15} W/cm^2) at $t = 1$ ps, and remain constant thereafter. The electron heat flux has been described in the code by a classical expression, which is saturated at the level $0.25 f n_e v_{Te} T_e$. Two different flux limiters $f = 0.08$ and 0.5 have been used in the calculations.

The radial temperature profiles obtained by the simple stationary model (4) and the more detailed CASTOR simulations are compared in Fig. 1. Parameters for this case include a peak laser intensity of 10^{15} W/cm^2, $\lambda_0 = 0.335\,\mu$m, and $n_e/n_c = 0.2$; the flux limiter f was set to 0.08. The radial temperature profile is shown at $z = 150\,\mu$m. A quasistationary radial temperature distribution is reached after approximately 10 ps, and no significant temperature change is observed thereafter. The simple analytical formula (5) slightly underestimates the maximum electron temperature and gradient. The reasons for this discrepancy are related to the simple (purely classical) model of the heat flux which exceeds locally the flux limit in numerical simulations by a factor of about 5 and to the distortion of the radial intensity profile in the course of propagation of the laser beam through the plasma. Both these effects can be accounted for through a refinement of the analytical model. However, this simple stationary model will give an adequate (within a few tens of a percent) estimate for the electron temperature that is used in the theoretical analysis below.

Figure 2 shows the temperature distribution in the interaction region for time $t = 15$ ps, and for the parameter set $I_{max} = 10^{14}$ W/cm^2, $\lambda_0 = 0.335\,\mu$m, $n_e/n_c = 0.2$, and initial ion and electron temperature 300 eV. This case involves strong inverse bremsstrahlung absorption of laser light. The resulting temperature contour plot shows a strong temperature gradient not only in the radial direction but also along the direction of propagation z. Effect of the heat flux inhibition is insignificant in this case. Our discussions of ion acoustic fluctuations in the next sections are based on the assumption of a strong temperature gradient only in the plane normal to the laser axis (cf. Fig. 3). However, Fig. 2 shows that for conditions found in laser plasma interaction experiments with strong absorption, we may expect a far more isotropic distribution for the temperature gradient and hence the ion acoustic turbulence spectra. The assumption of a radial temperature gradient is more appropriate for less dense plasmas as is seen in Fig. 3.

The reasonable agreement between the analytical model and numerical simulations (cf. Fig. 1) is mainly related to the fact that the short wavelength ($\lambda_0 = 0.335$ μm) laser radiation has been used and therefore the plasma was relatively dense and collisional. Much stronger nonlocal effects are obtained with long wavelength ($\lambda_0 = 1.06$ μm) laser radiation. Figure 3 shows a typical temperature profile that is calculated at the time $t = 7.6$ ps with a flux inhibition factor $f = 0.08$. The electron temperature grows with time and reaches a maximum value which is approximately two times larger than predicted by Eq. (5). A quasistationary temperature profile is established after approximately 10 ps. As is seen from the contour plot, the electron temperature in the axial direction is approximately constant because of small laser light absorption by the very underdense plasma.

In this case of 1 μm irradiation we have investigated

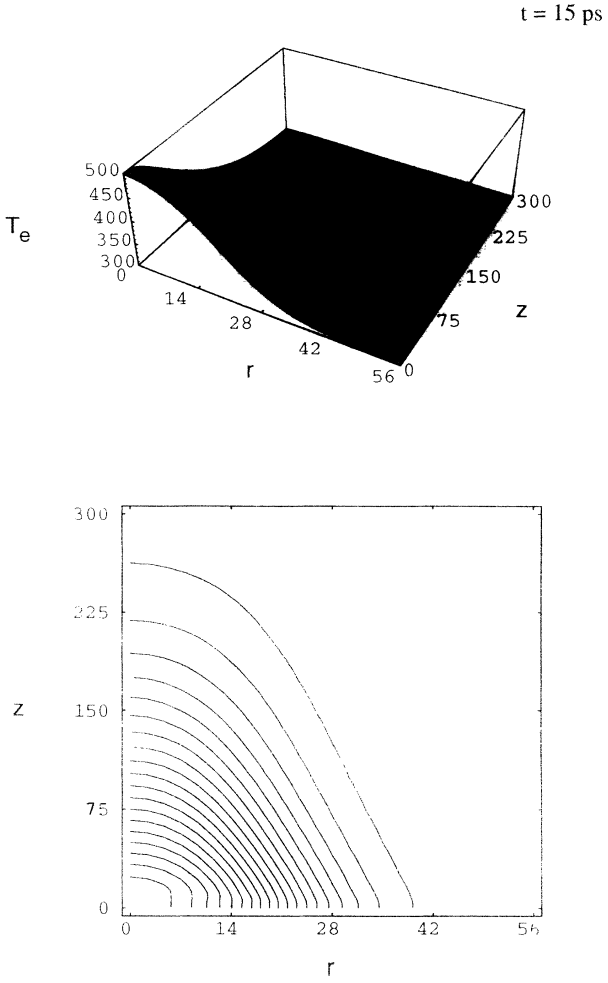

FIG. 2. Typical electron temperature profiles obtained from CASTOR simulations at time moment $t = 15$ ps. The carbon plasma was assumed to be 300 μm long and have initial ion and electron temperatures of 300 eV and electron density $n_e/n_c = 0.2$. The plasma was heated by a 0.335 μm wavelength laser focused at the center of the plasma column. A Gaussian radial beam profile was used with a vacuum FWHM diameter of 50 μm at the focal spot. The laser intensity was assumed to grow linearly from zero to the maximum value (10^{14} W/cm^2) at $t = 1$ ps, and then remain constant thereafter. The flux limiter was set to 0.08. The cylindrical coordinates (r, z) are expressed in μm, temperature T_e is given in eV.

the effect of an electron heat flux inhibition more carefully, because of the significant deviation of the electron temperature from the analytical prediction. The cross sections of the electron temperature radial distribution at the center of the plasma column, $z = 150\,\mu$m, are shown in Fig. 4 for the same conditions as in Fig. 3 for two flux limiter parameters $f = 0.5$ and 0.08. The stationary model of classical heat conductivity predicts an electron temperature that is smaller by 20% as compared to results of calculations with a moderate flux limiter $f = 0.5$. The decrease of f does not significantly affect the temperature distribution [cf. Fig. 4(a)], but does have a considerable effect on the magnitude of the electron heat flux which is decreased by almost four times [cf. Figs. 4(b) and 4(c)]. This effect makes the excitation of the return current instability more difficult to achieve. Dash-dot curves in Figs. 4(b) and 4(c) demonstrate the instability threshold, $q_{th} = \frac{5}{3} n_e c_s T_e$, calculated from the corresponding temperature distributions shown in Fig. 4(a). We see that instability can be excited almost in the entire plasma column for the moderate flux limiter case, $f = 0.5$. In the case of very strong inhibition ($f = 0.08$) the heat flux is much closer to the instability threshold, but it can still produce growth of IAW's at the perimeter of the laser beam.

Our hydrodynamical calculations confirm the predictions of the analytical theory for a collisional plasma case and demonstrate that the instability threshold conditions can be satisfied even with strong heat flux inhibition. (Note that our flux limiter $f = 0.08$ corresponds to the saturation of the heat flux at the level $0.02 n_e v_{Te} T_e$ which

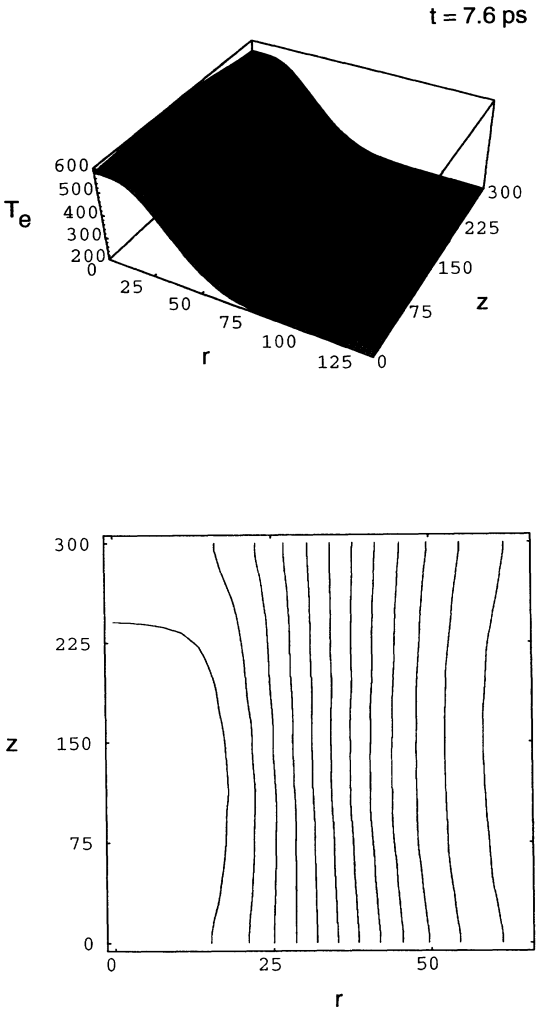

FIG. 3. Electron temperature profile and the contour plot obtained from CASTOR simulations at the time moment $t = 7.6$ ps. The initial ion and electron temperatures were 200 eV and electron density $n_e/n_c = 0.1$. The plasma was heated by a 1.06 μm wavelength laser with intensity 10^{15} W/cm^2. Other conditions are the same as in Fig. 2.

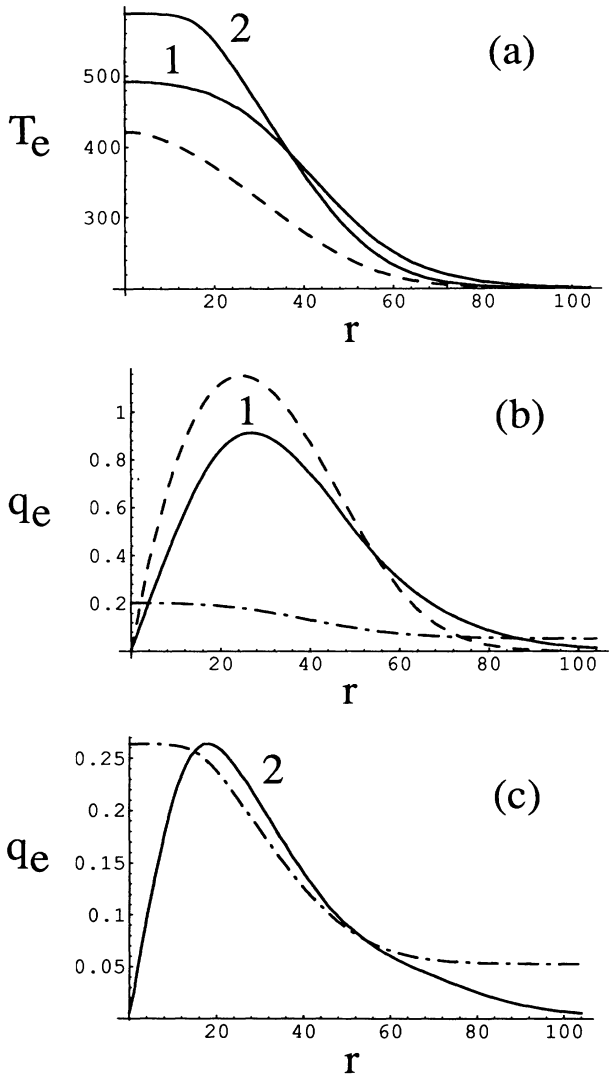

FIG. 4. The electron temperature (a) and electron heat flux [(b) and (c)] distribution in the center of the plasma column, $z = 150\,\mu$m, for the parameter set shown in Fig. 3 at time moment $t = 7.6$ ps. Curves 1 and 2 correspond to the flux limiter $f = 0.5$ and 0.08, respectively. Dashed curves correspond to the result obtained using the classical heat conductivity in the stationary limit. Dash-dot curves demonstrate the threshold heat flux for the excitation of return current instability.

is much lower than is usually assumed.) In the comparison of the classical heat flux approximation with results of the hydrodynamic simulations with both strongly inhibited and free streaming values of the heat flux, we have seen differences in temperature profiles and electron heat fluxes. However, the main feature of the plasma reference state, i.e., the heat flux above the threshold value for the return current instability, has been adequately characterized by the classical heat transport model. A full kinetic treatment is necessary in order to more accurately describe the threshold conditions for the instability in the regime of nonlocal heat conductivity. In this paper we have used results from several hydrodynamic runs with different flux limiters and our analytical theory to establish the existence of unstable plasma conditions. The analysis of the growth rate, however, is based on the phenomenological theory [16] of ion acoustic waves, which includes the nonlocal effects in the electron thermal transport.

III. THE CHARACTERISTICS OF THE ION ACOUSTIC TURBULENCE

It is well known that an ion acoustic turbulence (IAT) produces enhanced electron collisionality (cf., e.g., review papers on this subject [13,14]). In particular, IAT can contribute to anomalous laser light absorption and thermal transport inhibition in laser produced plasmas (cf., e.g., Ref. [20]). Since the introduction of short wavelength lasers in laser fusion experiments, classical collisioniality has dominated both absorption and transport processes. In addition, low levels of IAT found in particle simulations have also contributed to the declining role of IAT as an important physical mechanism in the laser fusion targets.

Our renewed interest in IAT has been motivated by the low threshold of the heat flux driven instability demonstrated in the preceding section analytically and numerically and difficulties encountered in the theoretical understanding of scattering instabilities, in particular SBS in recent experiments. Some of these problems have become more apparent with the recent progress in experimental techniques, in particular with the use of short laser pulses in scattering experiments [21]. It has become obvious that high levels of initial IAW fluctuations are required and perhaps different instabilities in addition to scattering processes, in order to quantitatively interpret SBS measurements [4].

In this section we adapt results of the weak turbulence theory for the heat flux driven ion acoustic instabilities [22,13,14] to the current conditions of laser plasma interaction experiments. The analytical results which are summarized below represent the actual level of theoretical understanding of these important, experimentally observed processes. The numerical values of the ion fluctuation levels are consistent with the enhancement of the acoustic noise, which is necessary to explain SBS measurements in laser produced plasmas. The characteristic time scales of growth and saturation of the instability are also compatible with the initial transient regime of laser plasma interaction experiments. The framework of a weak turbulence theory is appropriate in studies of a heat flux driven instability which excites a broad spectral range of uncorrelated ion acoustic modes under conditions of relatively weak drive and low fluctuation levels. We start by estimating the characteristic time scales of IAT growth and saturation and follow with estimates of the fluctuation levels and angular distributions in the stationary regime.

The linear growth rate of the kinetic instability driven by the electron heat flux depends on the wave number k and the heat flux q (cf. Ref. [16])

$$\gamma_{IA}(\vec{k}) = \gamma_s(k)\left(1 + \frac{3}{5}\frac{q\cos\delta_{\vec{k}}}{n_e T_e c_s}\right), \tag{7}$$

where $\gamma_s(k) = kc_s(\pi Zm_e/8m_i)^{1/2}$ is the electron Landau damping rate of the ion acoustic wave, and $\delta_{\vec{k}}$ is the angle between the wave vector $\vec{k}$ and the direction of a local temperature gradient. We have neglected contributions from ion Landau damping in Eq. (7) by assuming $ZT_e/T_i > 10$. The acoustic waves which would participate in resonance Brillouin scattering are characterized by wave numbers k of order $k_0 = \omega_0/c$, where the exact value depends on the direction of scattering. The growth time of these waves $\tau_1 \approx 1/\gamma_{IA}(k_0)$ is usually shorter than 1 ps for typical conditions found in laser plasma interaction experiments. The thermal flux driven instability occurs for the collisionless electrons, i.e., when the wavelength of the unstable mode is smaller than the electron mean free path λ_e. Therefore the linear growth expression (7) is valid for the relatively hot and underdense plasmas, when

$$v_{Te}/c > \nu_{ei}/\omega_0. \tag{8}$$

We have also neglected the effect of ion-ion collisions in Eq. (7), which can effectively stabilize IAW's with small wave numbers $k < k_2$. According to Ref. [16], the limiting value k_2 of the unstable region reads

$$k_2 = \frac{T_i}{ZT_e}\sqrt{\frac{m_i}{Zm_e}}\frac{\nu_{ii}n_eT_e}{q}, \tag{9}$$

where ν_{ii} is the ion-ion collision frequency. Relation (9) is valid for the relatively small heat fluxes (cf. Ref. [9]) where

$$q \lesssim n_eT_ec_s(m_i/Zm_e)^{1/2}(T_i/ZT_e)^{5/2}. \tag{10}$$

A detailed analysis of the IAW damping by ion collisions [16] leads to several regimes for the linear growth of the instability including a strong heat flux limit. In the present paper we will discuss the simpler case defined by Eqs. (9) and (10).

The nonlinear evolution of the kinetic instability of an IAW, driven by a constant electric field and/or return current induced by the electron heat flux, proceeds as follows [13,14]. The initial exponential growth, described by (7), continues until collective fluctuations have sufficient amplitude to significantly modify the particle distribution function. From the macroscopic point of view,

enhanced fluctuations increase the anomalous resistivity $\eta = m_e\nu_{an}/n_e e^2$, and slow the initial electron-ion drift. The drift velocity $u_d \approx q/n_e T_e$ describes a return current of cold electrons, $j_e = en_e u_d$, which is a source of instability when $u_d \geq c_s$. The quasilinear theory [13,14] leads to the following expression for the turbulent electron collision frequency:

$$\nu_{an} = \frac{2}{n_e m_e u_d^2} \int \frac{d^3k}{(2\pi)^3} \vec{k} \cdot \vec{u}_d(t) \gamma_{IA}(\vec{k},t) N(\vec{k},t), \quad (11)$$

where the IAW quanta $N(\vec{k},t)$ are defined in terms of the wave energy spectral density W_k and ion acoustic frequency ω_s, $N(k,t) = W_k/\omega_s$. The increased collisionality (11) is responsible for the transient evolution of the spectra, which includes electron heating, acceleration of ions and the decay of fluctuations from their maximum value, at the moment of first saturation, toward asymptotic values in the stationary regime. During the decay of IAT, the anomalous Joule heating of electrons and the production of fast ions continues. In the stationary stage, the particle distribution function is close to marginal stability and the primary mechanism that is responsible for the spectral energy distribution is induced scattering by ions.

The characteristic time scale t_{sat} of the temporal evolution of IAT before the fluctuations reach the stationary stage is related to the linear growth rate (7). In particular, for conditions close to threshold and for a wave number $k \approx \omega_0/c$, we can estimate the characteristic saturation time t_{sat} as

$$t_{sat} \approx \omega_0^{-1} \frac{c}{c_s} \sqrt{\frac{m_i}{Zm_e}}. \quad (12)$$

For the typical experimental conditions, this saturation time can be of the order of few ps. We will be more specific in the calculation of t_{sat} below, by giving the full range of values for different wave numbers in the case of weakly and strongly driven instabilities.

In the nonlinear quasistationary stage of the instability the induced scattering of an IAW by ions [13,14] leads to the following distribution of the ion acoustic quanta $N(\vec{k})$ in the Fourier space:

$$N(\vec{k}) = N_{KP}(k)\Phi(\cos\delta_{\vec{k}}), \quad (13)$$

where $N_{KP}(k)$ is the Kadomtsev-Petviashvili frequency spectrum [23]

$$N_{KP}(k) = 4\pi n_e m_i \frac{T_e}{T_i} \frac{\gamma_s(k)}{k^5} \ln\frac{1}{k\lambda_{De}}. \quad (14)$$

This formula is valid for wavelengths $\lambda_{De}^{-1} > k > k_{min}$, where the minimum wave number $k_{min} \sim k_2$ [cf. Eq. (9)] defines the position of the maximum of the turbulence spectrum. For smaller wave numbers, ion-ion collisions suppress the instability and cause a rapid decrease of $N(k)$ toward zero for $k < k_{min}$.

The general solution for IAW quanta $N(\vec{k})$, described by Eqs. (13) and (14), is valid for the wide range of values of the ambipolar electric field E which gives rise to the return current of cold electrons. The particular form of the function Φ (13), however, depends on the characteristic parameter $K_N = E/E_{NL}$. The limiting value of the electric field

$$E_{NL} = \frac{m_e}{6e\pi} c_s \omega_{pi} \frac{ZT_e}{T_i}$$

separates weakly driven IAT from the strongly driven case, where induced scattering on ions plays an essential role in producing IAT spectra. The parameter K_N, the so called turbulent Knudsen number (cf. Refs. [14,22]), can be expressed in terms of the temperature gradient from the condition of the zero total electric current, i.e., $eE \approx \nabla(n_e T_e)/n_e$.

$$K_N \approx 6\pi \frac{v_{Te}^2}{c_s\omega_{pi}} \frac{T_i}{ZT_e} |\vec{\nabla} \ln T_e|, \quad (15)$$

One can obtain a simple estimate for the parameter K_N from the stationary plasma heating model of Sec. II A. By combining Eqs. (5) and (6) with the definition of the classical heat flux we obtain $|\vec{\nabla}T_e| \approx 0.25T_0/a$, and the following simple expression for the turbulent Knudsen number (15) is obtained:

$$K_N \approx 280 \frac{v_{Te}}{a\omega_{pi}} \frac{T_i}{ZT_e}.$$

Typically K_N varies between 0.1 and 10 for parameters found in current laser plasma interaction experiments.

The function Φ (13) describes the angular distribution of the IAT spectra with respect to the direction of a local temperature gradient. It has nonzero values for $\delta_{\vec{k}} < \pi/2$ and is given by the following expressions [13,14]:

$$\Phi(\xi) = \begin{cases} \frac{4K_N}{3\pi\xi} \frac{d}{d\xi} \frac{\xi^4}{1-\xi+\epsilon} & \text{if } K_N \ll 1 \\ \sqrt{K_N} \frac{19.8}{\pi} \xi^2 (1 + 1.8 - 2\xi^4) & \text{if } K_N \gg 1, \end{cases} \quad (16)$$

where $\epsilon \approx K_N \ln(1/K_N)$ for $K_N \ll 1$. In the case of weakly driven IAT ($K_N \ll 1$) the angular distribution of IAT spectra is peaked in the direction of the temperature gradient (cf. Fig. 5). For $K_N \gg 1$, Φ becomes more isotropic (cf. Fig. 6) and displays weak maxima at $\delta_{\vec{k}} \approx \pm 35°$. For both weakly and strongly driven turbulence, the function $\Phi(\xi)$ decays rapidly to zero at $\delta_{\vec{k}} \approx \pm 90°$, i.e., for the ion waves propagating in a direction normal to the temperature gradient.

Figure 5 shows the the spectral distribution of the ion acoustic quanta $N(\vec{k})$ (13) normalized to the thermal equilibrium values $N_{eq} = T_e/kc_s$ in a logarithmic scale. Figure 5 corresponds to small K_N and Fig. 6 to large values of the parameter K_N [cf. Eq. (16)]. The main parts of both figures are the contour plots with the thin solid lines identified by numbers indicating the orders of magnitude of IAT enhancement above the thermal level. The angle $\delta_{\vec{k}}$ measures the direction of the wave vector $\vec{k}$ with respect to the direction of a temperature gradient. The turbulence spectra are strongly enhanced

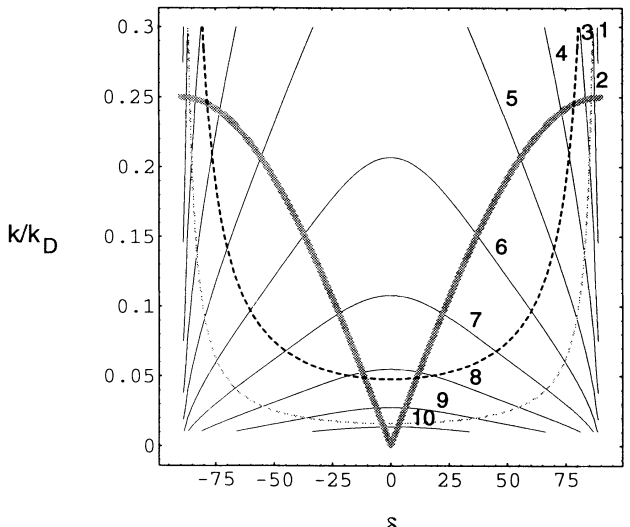

FIG. 5. The contour plot of a logarithm of the normalized ion density fluctuations $kc_sN(\delta_{\vec{k}})/T_e$ (13) as a function of the wave number and the angle $\delta_{\vec{k}}$ between temperature gradient and the wave vector $\vec{k}$. The turbulence parameter K_N (15) equals 0.5. Numbers near solid lines define orders of magnitude for ion fluctuations above the thermal level. Two dotted curves define the range of wave vectors being enhanced on the time scale τ (17) of 10 ps (darker dashed curve) and 30 ps (lighter dashed curve). The thick gray lines denote the ion waves which can participate in the Brillouin scattering (four different examples of interaction are shown in Fig. 7), if the temperature gradient is perpendicular to the beam axis. The rest of the plasma parameters are $n_e = 10^{20}$ cm^{-3}, $T_e = 800$ eV, $ZT_e/T_i = 12$, and $n_e/n_c = 0.1$.

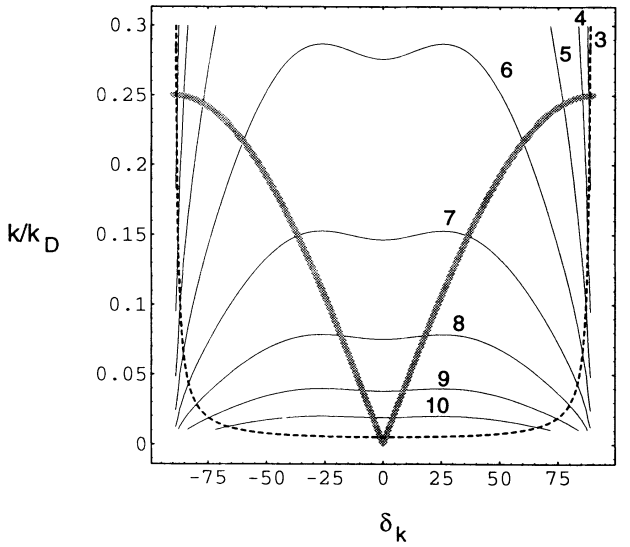

FIG. 6. The contour plot of a logarithm of the normalized ion density fluctuations $kc_sN(\delta_{\vec{k}})/T_e$ (13) as a function of the wave number and the angle $\delta_{\vec{k}}$ between temperature gradient and the wave vector $\vec{k}$. The turbulence parameter K_N (15) equals 5. The rest of the parameters are as in Fig. 5.

in the direction of the temperature gradient and become zero for $\delta_{\vec{k}} = \pm 90°$. The maximum of N is reached at $k = k_2$ (9), which defines the cutoff due to ion collisions in our model. The smaller the wave numbers, however, the longer the time of growth and saturation of IAW instability. We have illustrated this point by drawing two dotted curves in Fig. 5. They correspond to two values of the characteristic time

$$\tau = 1/\gamma_{IA}(\vec{k}), \tag{17}$$

where the linear growth rate γ_{IA} is defined by Eq. (7). The upper curve (darker dashed line) corresponds to $\tau =$ 10 ps and the lower curve (lighter dashed line) is defined by $\tau = 30$ ps. They describe the lower bounds for the region of wave vectors, which can be enhanced and reach the stationary state on time scales of 10 ps and 30 ps, respectively. While solving Eq. (17) for k as a function of $\delta_{\vec{k}}$, at these two specific times, we have expressed the heat flux q [cf. Eq. (7)] in terms of the turbulence parameter K_N (15). The result has the following form:

$$\frac{k}{k_D} = 0.33\,\frac{\ln\Lambda\lambda_0}{\tau\zeta(Z)K_N T_e^{3/2}\cos(\delta_{\vec{k}})}\,\frac{T_i}{T_e}, \tag{18}$$

where τ is in ps, T_e in keV, and λ_0 in μm. Expression (18) is sensitive to the value of K_N and shows that for small values of K_N one is less likely to observe strong enhancement (magnitude of the order of 10) in the short time scale of the initial transient heating of a plasma. This restriction is less important for large K_N as is demonstrated by plotting (18) for $\tau = 10$ ps in Fig. 6. The thick gray lines in Fig. 4 show the location of wave vectors satisfying resonance conditions for the SBS. We will discuss the effect of nonthermal ion fluctuations on the scattering instabilities in the next section.

In summary, the analysis of return current driven ion acoustic turbulence shows that high fluctuation levels can be excited on time scales corresponding to the initial transient heating of the plasma. This includes the short pulse, 10 ps interaction experiments. Ion acoustic fluctuations are localized predominantly in the radial plane and are directed toward the laser axis. The angular distribution of enhanced wave vectors along the direction of the temperature gradient is relatively wide so that intense ion fluctuations are predicted up to angles $\delta_{\vec{k}} \sim 70° - 80°$. Manifestations of these fluctuations include enhanced absorption and scattering of the electromagnetic waves in the laser-produced plasma.

IV. LASER LIGHT SCATTERING FROM THE ION ACOUSTIC TURBULENCE

The interaction of a laser beam with density fluctuations produces scattered electromagnetic waves. The weak turbulence theory provides the following expression for the intensity of the scattered radiation [14,16]:

$$\nabla \frac{dI_B}{d\Omega_{\vec{n}}\, d\omega} = \frac{(\vec{e}\cdot\vec{e}_0)^2 I_0}{16\pi^2 n_c T_e}\frac{n_e}{n_c} k_0^4 k_s c_s [N(\vec{k}_s)\,\delta(\omega-\omega_0-k_s c_s) + N(-\vec{k}_s)\,\delta(\omega-\omega_0+k_s c_s)], \quad (19)$$

where $\vec{k}_s = k_0(\vec{n}_0 - \vec{n})$ is the wave vector of the ion acoustic wave participating in the scattering, the unit vectors $\vec{n}_0$ and $\vec{n}$ represent the directions of propagation of the primary and scattered electromagnetic waves, $\vec{e}_0$ and $\vec{e}$ are their polarization vectors, respectively, and $d\Omega_{\vec{n}}$ is the solid angle in the direction of the scattered wave propagation. The scattering geometry shown in Fig. 7 shows that the length of the vector $k_s = 2k_0 \sin(\psi/2)$ depends on the scattering angle ψ and in the case when the temperature gradient is perpendicular to the laser beam axis it is directly related to the ion acoustic wave propagation angle $\delta_{\vec{k}} = \psi/2$.

Equation (19) predicts two spectral components of the scattered light: Stokes (redshifted) and anti-Stokes (blueshifted), corresponding to the decay and coalescence of the pump and ion acoustic waves, respectively (cf. Fig. 7). Their directions of propagation defined by vectors $\vec{k}_r$ (Stokes—redshifted light) and $\vec{k}_b$ (anti-Stokes—blueshifted light) are different because of the anisotropy of ion density fluctuations. The Stokes component is radiated in the directions of unit vectors $\vec{n} \parallel \vec{k}_r$, which satisfies the relation $(\vec{n}_0 - \vec{n})\cdot\vec{\nabla}T_e > 0$. Correspondingly, directions of anti-Stokes emission satisfy the opposite inequality. The wave vectors of ion acoustic modes $\vec{k}_s$, which are shown in Fig. 7, correspond to thick gray lines in Figs. 5 and 6—the negative angles δ_k define ion waves participating in an anti-Stokes interaction while the positive δ_k values relate to waves contributing to a Stokes interaction.

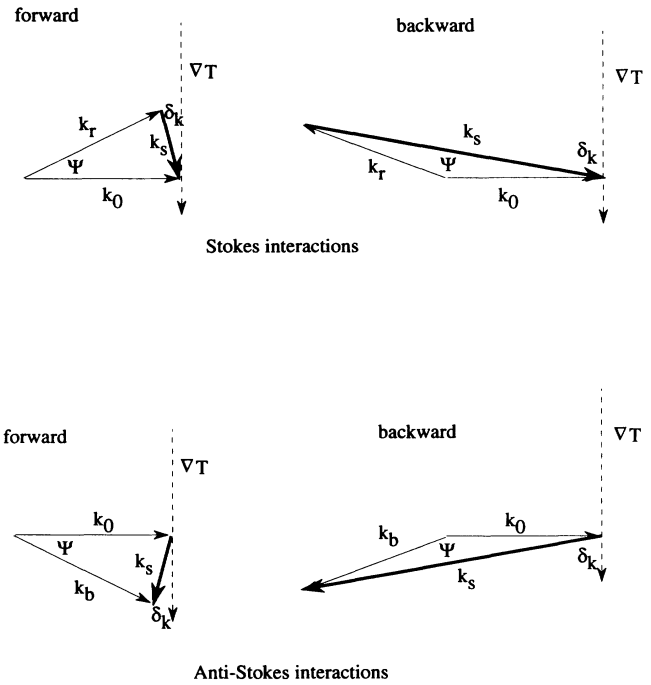

FIG. 7. Four examples of different wave interactions corresponding to Brillouin scattering. Thick arrows described as $\vec{k}_s$ correspond to ion sound waves. Electromagnetic waves: pump k_0 and scattered light $\vec{k}_r$ (redshifted or Stokes components) or k_b (blueshifted or anti-Stokes component) form the angle Ψ. Angle $\delta_{\vec{k}}$ between the directions of temperature gradient ∇T and vectors $\vec{k}_s$ correspond to the variable of Figs. 5 and 6.

The qualitative picture of ion acoustic turbulence and the interaction geometry is represented in Fig. 8. We have assumed that the laser beam has a smooth intensity profile and that its absorption in the plasma is not too strong. The contours of equal temperature are parallel to the direction of laser propagation and the temperature gradient points towards the laser beam axis. The shaded regions correspond to the ion acoustic turbulence which is excited at the periphery of the beam, where the temperature gradient reaches maximum values. The wave vectors of the ion acoustic fluctuations exist within a wide cone of angles centered along the direction of the temperature gradient (cf. Figs. 5 and 6). Figure 8 shows the basic geometry of localized plasma heating and of the excitation of the ion acoustic turbulence. It illustrates an idealized situation, which can be easily altered for example by increased absorption. In Sec. II B we have shown examples of strongly absorbing plasmas, where temperature gradients (cf. Fig. 2) change direction from being normal to the laser axis to being antiparallel to the direction of beam propagation. Obviously, the corresponding distribution of ion acoustic turbulence will cover an angular range which is much wider than the distribution corresponding to Fig. 8. Similarily, in realistic plasmas, the location and orientation of the hot intensity region is affected by plasma response and should result in a far more isotropic distribution of ion acoustic turbulence as compared to the ideal example shown in Fig. 8. Our model of plasma heating and excitation of ion acoustic turbulence (Fig. 7) shows the strongest enhancement for nearly forward scattering. It involves ion waves with small wave numbers, which are most strongly enhanced (cf. Fig. 4) and which propagate closely to the direction of the temperature gradient. On the other hand, the growth rate of small wave number ion waves is the smallest [24] and it may take a much longer time than the characteristic transient of the initial heating to reach the stationary regime described by the Kadomtsev-Petviashvili spectrum (14).

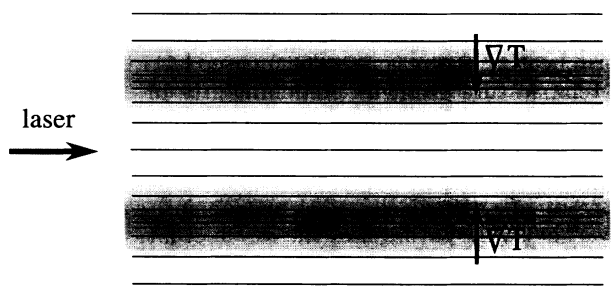

FIG. 8. The schematic diagram of the constant temperature lines based on the results of numerical simulations shown in Fig. 3. Ion acoustic turbulence is excited in the shaded regions around the laser beam axis.

If the temperature gradient is exactly perpendicular to the laser beam axis then the sound waves contributing to the backscattered Brillouin scattering experience the smallest enhancement (cf. Figs. 5 and 6). However, they still can be a few orders of magnitude above thermal levels (e.g., for $\psi \approx 170°$). In more realistic plasma geometries and for different directions of the temperature gradient (cf., e.g., Figs. 2 and 3) backscattered Brillouin can also be strongly enhanced.

In order to obtain quantitative estimates of the scattered light, Eq. (19) can be integrated over the frequency and written as

$$\frac{dI_B}{d\Omega_{\vec{n}}} \approx 1.8 \times 10^{-8} I_0 \frac{l}{\lambda_0^2} \frac{n_e}{n_c} \left(1 - \frac{n_e}{n_c}\right)^2 \frac{k_s c_s N(\vec{k}_s)}{T_e}, \quad (20)$$

where the scattering length l and the laser wavelength are in micrometers. The last factor in this expression is the ratio of the enhanced ion acoustic fluctuations to the thermal noise level. Therefore the numerical coefficient in the front of (20) corresponds to the thermal scattering. The enhancement factor can be directly evaluated from Eqs. (14) and (16). The particular example relevant to the conditions of the experiment [3] is shown in Fig. 5. The resonance conditions are satisfied along the thick gray lines. One can see that the Brillouin scattering could be very effective in the forward direction and could provide an increase of the angular divergence of the transmitted beam by 10°–15°. The amplification of the scattered light in the near backward direction can also be significant with values of 5–6 orders of magnitude above the thermal level. These temperature induced ion density fluctuations may also serve as the enhanced initial noise for the stimulated Brillouin scattering, if the SBS amplification coefficient is greater than 1. When the stimulated instability takes place the redshifted component of the scattered light spectra should dominate, contrary to the case of scattering from the enhanced ion fluctuations when both blueshifted and redshifted components are of similar intensity.

V. DISCUSSION AND SUMMARY

We have discussed in detail a mechanism for enhancement of ion fluctuations above thermal levels in laser produced plasmas. This mechanism is based on the heat flux driven ion acoustic instability produced by the nonuniform heating of a plasma. The focused laser beam creates a temperature gradient predominantly in the direction perpendicular to the laser axis. The temperature gradient that forms on the short time scale of the initial heating phase is responsible for the development of a return current of thermal electrons and an ion wave instability. The saturated level of the ion fluctuations and their angular distribution have been estimated from the weak turbulence theory. We have also discussed properties of Brillouin scattering from these fluctuations.

Our study has been motivated by extensive experimental evidence implying a nonequilibrium state of laser plasmas, which is characterized by large levels of electrostatic fluctuations. This has been demonstrated most convincingly in the measurements of stimulated Brillouin scattering in preformed plasmas (cf. Refs. [3,7]). Also nonthermal levels of ion acoustic fluctuations have been observed in short pulse scattering experiments [3,4] suggesting that the process responsible for the enhancement must operate on picosecond time scales. The initial nonuniform heating of the plasma is identified in our work as a potential source of ion instability. This is the most basic and universal process taking place in all laser plasma interaction experiments.

In the final discussion of our results we would like to point out two additional applications of ion acoustic turbulence. First we will discuss the effect of random phase plate optics on the generation of ion fluctuations. We then show how ion turbulence can increase the damping on the electromagnetic wave scattered by stimulated Raman instability, particularly in the vicinity of the quarter critical density.

A. Excitation of ion acoustic fluctuations by the RPP laser beam

Our results can also be applied to randomized laser beams with small scale spatial modulations in their intensity. In that case, ion acoustic turbulence can be excited not only at the periphery of the laser beam, but in the whole interaction region. The statistical theory of the RPP optics [25] together with the results presented in previous sections can be used to evaluate threshold conditions of the ion acoustic instability. Formulas (5) and (6) can be applied to the whole laser beam as well as to individual hot spots. We will discuss two different limits of plasma heating by RPP beams. The first and simple case assumes that transient heating takes place within a single hot spot with no increase of temperature outside the high intensity region. This may be of relevance to RPP optics with time varying location of the hot spots produced, for example, by the induced spatial incoherence effects. The second case, which is relevant for a stationary intensity distribution, assumes only a small temperature difference δT_e between the hot spot region and surrounding plasma.

According to the statistical theory of laser fluctuations [25], the hot spot power P_{hot} is directly related to the intensity of the hot spot I_{hot} and its cross section $\pi(F\lambda_0)^2$, where F is the focal number of the focusing optics (the ratio of the characteristic diameter of the incident laser beam to the focal length). Therefore we can apply the probability function $p(I) \approx (4I/\bar{I}^2)\exp(-2I/\bar{I})$ of the hot spot intensity distribution derived in [25] and estimate the average fluctuation of the power

$$\langle \delta P \rangle = \sqrt{\langle (I_{hot} - \bar{I})^2 \rangle} \pi (F\lambda_0)^2$$

which gives us $\langle \delta P \rangle \approx P_0 (F\lambda_0/a)^2$, where a represents the whole laser beam radius in the plasma and P_0 corresponds to the average power of the laser beam.

By using $\langle \delta P \rangle$ as P_{hot}, we can rewrite the threshold condition for the ion wave instability (6) for the single

hot spot. As the beam diameter a in Eq. (6) is now replaced by $F\lambda_0$, the short scale temperature variations can result in lower threshold in spite of the smaller power that is contained in the single hot spot. The new threshold that is related to the single hot spot is lower by factor $(F\lambda_0/a)^{1/5}$ as compared to the value obtained for the whole beam. This result is relevant to the first case mentioned above when the heating takes place in localized hot spots without change to the background temperature of the plasma. It suggests a uniform distribution of ion acoustic turbulence particularly for a large number of hot spots.

For the second case, when the temperature is weakly disturbed as compared to background plasma, we have from (5) that $\delta T_e/T_0 \approx \frac{1}{5}\delta P/P_0$. By evaluating the heat flux fluctuation $\delta q \sim \zeta(Z) n_e v_{Te}^2 \nu_{ei}^{-1} \delta T_e/F\lambda_0$, we see that the threshold condition for the onset of the ion acoustic instability is now increased by a factor $5a/F\lambda_0$ as compared to the value obtained in Sec. II A. The threshold can be written as

$$F > a^2/2\zeta\lambda_e\lambda_0,$$

where Eq. (5) should be used to evaluate the electron mean free path λ_e. Usually the right hand side of this inequality is more then 10, making the threshold of ion wave instability relatively high, unless plasma temperature is in the range of 2–3 keV. In this case the mean free path is long and the threshold becomes lower.

B. Effect of ion acoustic turbulence on the Raman scattering

The enhanced short wavelength ion acoustic fluctuations increase damping on the electromagnetic waves propagating in the plasma. This anomalous absorption process is characterized by the effective damping coefficient of the wave with frequency ω [26,27,14]

$$\nu_{eff}(\omega) = \frac{\omega}{2}\int \frac{d\vec{k}}{(2\pi)^3}\frac{kc_s N(\vec{k})}{n_e T_e}\mathrm{Im}\frac{1}{\epsilon_L(\omega,\vec{k})}\cos^2\varphi_{\vec{k}}, \quad (21)$$

where $\epsilon_L(\omega,\vec{k})$ is the plasma dielectric function and $\varphi_{\vec{k}}$ stands for the angle between the direction of the electric field of the electromagnetic wave and the ion acoustic wave vector. Because of the resonance character of the dielectric function ϵ_L, anomalous absorption is effective for waves with frequencies ω comparable to the electron plasma frequency and certainly smaller than $1.4\,\omega_{pe}$ [27]. Also, the most effective contribution to Eq. (21) is due to the ion waves propagating along the electric field of the electromagnetic wave, i.e., perpendicularly to the direction of propagation of the laser pump. This is exactly the direction of the strongest enhancement predicted by Eq. (13) for $N(\vec{k})$. An experimental situtation where the anomalous damping of the electromagnetic waves can be particularly important is stimulated Raman scattering (SRS) in the vicinity of the the quarter critical density $n_c/4$. Stimulated Raman scattering produces electromagnetic waves of frequencies ω, which correspond to maximum values of ν_{eff} (21) at $n_e \leq n_c/4$ (cf. Ref. [28]). Thus our scenario of an ion acoustic instability due to localized plasma heating may provide the natural explanation of the so called Raman gap—unusual suppression of SRS reflectivity for $0.2 < n_e/n_c < 0.25$ observed in many experiments.

C. Summary

An analysis of the properties of ion acoustic turbulence produced in a preformed plasma due to intensity inhomogeneities of an incident Gaussian-like laser beam has resulted in theoretical predictions which are consistent with many experimental results. We have identified a basic and common process taking place during laser plasma interactions, i.e., transient nonuniform heating of electrons, and have linked this to a few unexplained features of such plasmas, for instance enhanced levels of ion acoustic fluctuations. These fluctuations can scatter electromagnetic radiation and produce Stokes and anti-Stokes Brillouin components or they provide nonthermal noise levels for the growth of stimulated Brillouin scattering. In addition, they can develop on the relatively short time scales, typically tens of picoseconds, and are therefore relevant in the interpretation of short pulse scattering experiments. Finally, the presence of enhanced ion acoustic fluctuations in laser-produced plasmas can have important consequences on the behavior of plasmas created by the RPP pumps and on the properties of other parametric instabilities such as stimulated Raman scattering.

ACKNOWLEDGMENTS

This work was partly supported by the NATO Collaborative Research Grant, and by the Natural Sciences and Engineering Research Council of Canada.

[1] W. L. Kruer, *The Physics of Laser Plasma Interactions* (Addison-Wesley, Reading, MA, 1988).

[2] V. T. Tikhonchuk, Usp. Fiz. Nauk **161**, 29 (1991) [Sov. Phys. Usp. **34**, 903 (1991)]; Kvant. Elektron. (Moscow) **18**, 151 (1991) [Sov. J. Quantum Electron. **21**, 133 (1991)].

[3] H. A. Baldis, D. M. Villeneuve, B. LaFontaine, G. D. Enright, C. Labaune, S. Baton, Ph. Mounaix, D. Pesme, M. Casanova, and W. Rozmus, Phys. Fluids B **5**, 3319 (1993).

[4] Ph. Mounaix, D. Pesme, W. Rozmus, and M. Casanova, Phys. Fluids B **5**, 3304 (1993).

[5] R. L. Berger, E. A. Williams, and A. Simon, Phys. Fluids B **1**, 414 (1989).

[6] A. A. Zozulya, V. P. Silin, and V. T. Tikhonchuk, Kvant. Elektron. (Moscow) **11**, 496 (1984) [Sov. J. Quantum

Electron. **14**, 339 (1984)].
[7] P. E. Young, H. A. Baldis, and K. G. Estabrook, Phys. Fluids B **3**, 1245 (1991).
[8] T. Kolber, W. Rozmus, V. T. Tikhonchuk, Ph. Mounaix, and D. Pesme, Phys. Rev. Lett. **70**, 1810 (1993).
[9] V. Yu. Bychenkov and V. P. Silin, Fiz. Plazmy **9**, 282 (1983) [Sov. J. Plasma Phys. **9**, 165 (1983)].
[10] D. W. Forslund, J. Geophys. Res. **75**, 17 (1970).
[11] J. S. DeGroot, W. L. Kruer, and H. A. Baldis (unpublished).
[12] H. A. Baldis, J. D. Moody, D.S. Montgomery, C. Labaune, S. Dixit, R. L. Berger, B. F. Lasinski, and K. Estabrook, in *Inertial Confinement Fusion Quarterly Report, Lawrence Livermore National Laboratory*, Vol. 3, p. 137 (unpublished).
[13] A. A. Galeev and R. Z. Sagdeev, in *Handbook of Plasma Physics*, edited by A.A. Galeev, and R. N. Sudan (North-Holland, Amsterdam, 1984), Vol. 2, p. 271.
[14] V. Yu. Bychenkov, V. P. Silin, and S. A. Uryupin, Phys. Rep. **164**, 119 (1988).
[15] V. Yu. Bychenkov and V. P. Silin, Pis'ma Zh. Eksp. Teor. Fiz. **44**, 42 (1986) [JETP Lett. **44**, 52 (1986)].
[16] V. Yu. Bychenkov, J. Myatt, W. Rozmus, and V. T. Tikhonchuk, Phys. Plasmas (to be published).
[17] E. M. Epperlein, Phys. Rev. Lett. **65**, 2145 (1990).
[18] A. V. Maximov and V. P. Silin, Pis'ma Zh. Eksp. Teor. Fiz. **58**, 264 (1993) [JETP Lett. **58**, 271 (1993)].
[19] R. Rankin, C. E. Capjack, and C. R. James, Phys. Fluids B **1**, 2437 (1989); R. Rankin, A. Birnboim, R. Marchand, and C. E. Capjack, Comput. Phys. Commun. **41**, 21 (1986).
[20] D. G. Colombant and W. M. Manheimer, Phys. Fluids **23**, 2512 (1980).
[21] H. A. Baldis, W. Rozmus, C. Labaune, Ph. Mounaix, D. Pesme, S. Baton, and V. T. Tikhonchuk, in *Laser Interaction with Atoms, Solids and Plasmas*, Vol. XX of *NATO Advance Study Institute Series, B: Physics*, edited by R. More (Plenum, New York, 1994).
[22] V. Yu. Bychenkov and V. P. Silin, Zh. Eksp. Teor. Fiz. **82**, 1886 (1982) [Sov. Phys. JETP **55**, 1086 (1982)].
[23] B. B. Kadomtsev, and V. I. Petviashvili, Zh. Eksp. Teor. Fiz. **43**, 2234 (1962) [Sov. Phys. JETP **16**, 1578 (1963)]; V. I. Petviashvili, Dokl. Akad. Nauk SSSR **153**, 1295 (1963) [Sov. Phys. Dokl. **8**, 1218 (1963)].
[24] M. D. Tracy, E. A. Williams, K. G. Estabrook, J. S. DeGroot, and S. M. Cameron, Phys. Fluids B **5**, 1430 (1993).
[25] H. A. Rose and D. F. DuBois, Phys. Fluids B **5**, 590, 3337 (1993).
[26] J. M. Dawson and C. Oberman, Phys. Fluids **5**, 517 (1962).
[27] R. J. Faehl and W. L. Kruer, Phys. Fluids **20**, 55 (1977).
[28] W. Rozmus, H. A. Baldis, and D. M. Villeneuve, Comments Plasma Phys. Controlled Fusion **12**, 1 (1988).

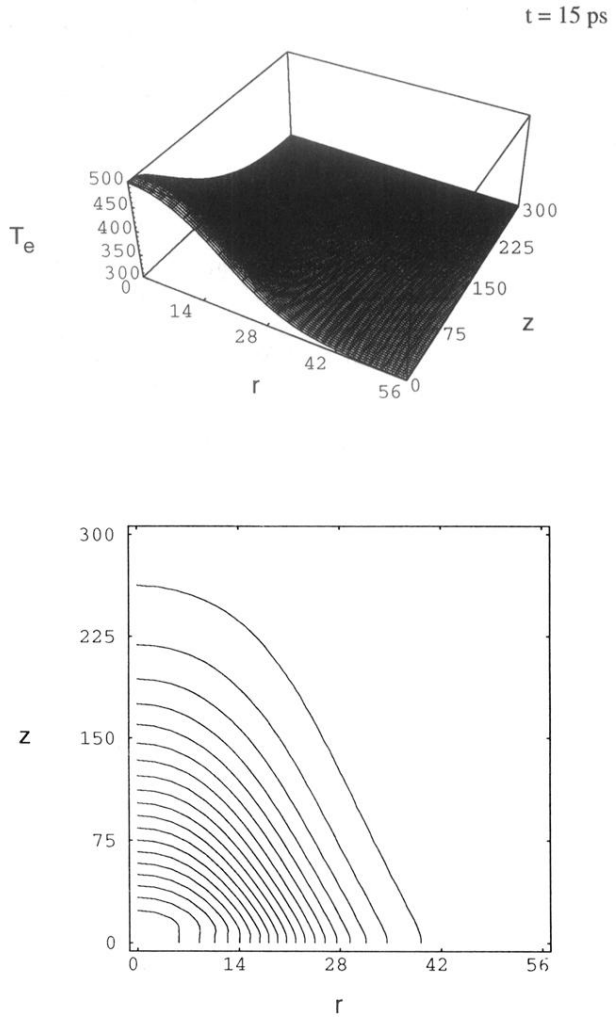

FIG. 2. Typical electron temperature profiles obtained from CASTOR simulations at time moment $t = 15$ ps. The carbon plasma was assumed to be 300 μm long and have initial ion and electron temperatures of 300 eV and electron density $n_e/n_c = 0.2$. The plasma was heated by a 0.335 μm wavelength laser focused at the center of the plasma column. A Gaussian radial beam profile was used with a vacuum FWHM diameter of 50 μm at the focal spot. The laser intensity was assumed to grow linearly from zero to the maximum value (10^{14} W/cm^2) at $t = 1$ ps, and then remain constant thereafter. The flux limiter was set to 0.08. The cylindrical coordinates (r, z) are expressed in μm, temperature T_e is given in eV.

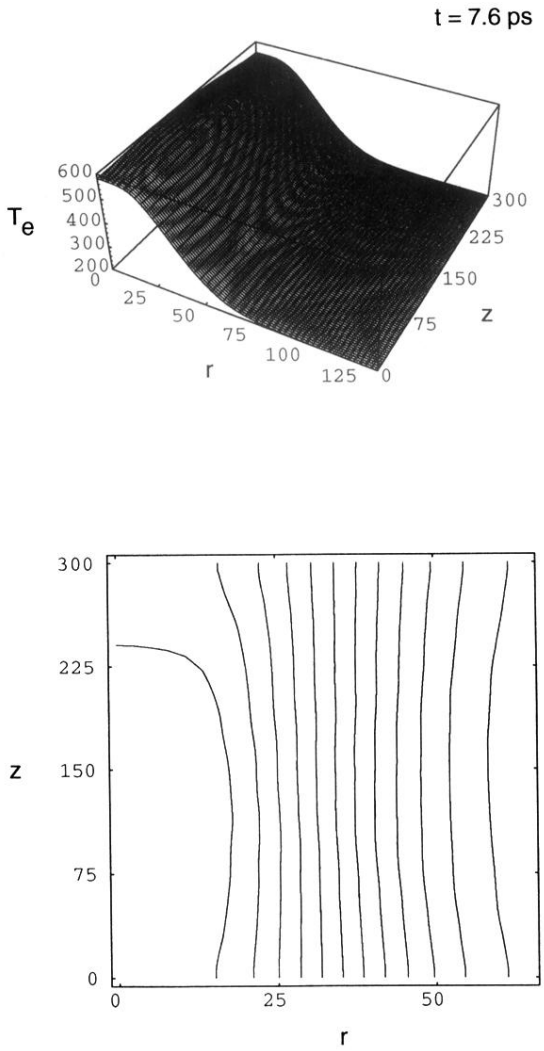

FIG. 3. Electron temperature profile and the contour plot obtained from CASTOR simulations at the time moment $t =$ 7.6 ps. The initial ion and electron temperatures were 200 eV and electron density $n_e/n_c = 0.1$. The plasma was heated by a 1.06 μm wavelength laser with intensity 10^{15} W/cm^2. Other conditions are the same as in Fig. 2.

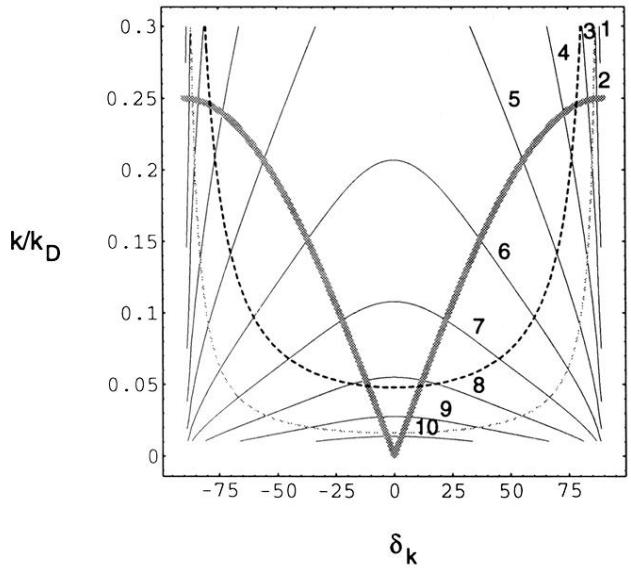

FIG. 5. The contour plot of a logarithm of the normalized ion density fluctuations $kc_sN(\delta_{\vec{k}})/T_e$ (13) as a function of the wave number and the angle $\delta_{\vec{k}}$ between temperature gradient and the wave vector $\vec{k}$. The turbulence parameter K_N (15) equals 0.5. Numbers near solid lines define orders of magnitude for ion fluctuations above the thermal level. Two dotted curves define the range of wave vectors being enhanced on the time scale τ (17) of 10 ps (darker dashed curve) and 30 ps (lighter dashed curve). The thick gray lines denote the ion waves which can participate in the Brillouin scattering (four different examples of interaction are shown in Fig. 7), if the temperature gradient is perpendicular to the beam axis. The rest of the plasma parameters are $n_e = 10^{20}$ cm^{-3}, $T_e = 800$ eV, $ZT_e/T_i = 12$, and $n_e/n_c = 0.1$.

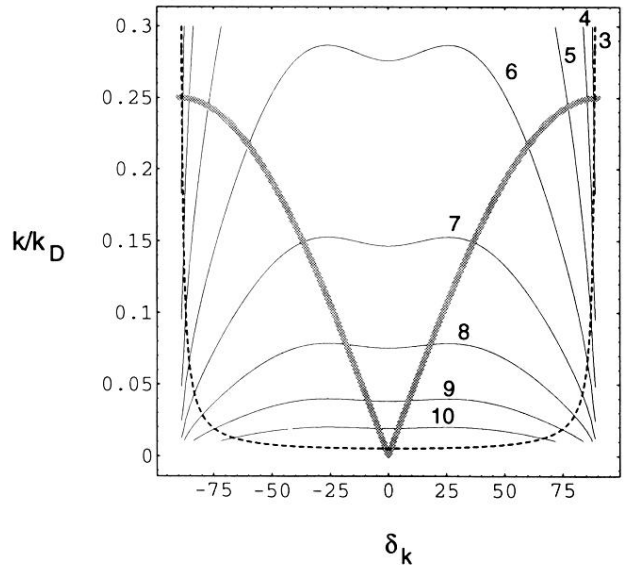

FIG. 6. The contour plot of a logarithm of the normalized ion density fluctuations $kc_s N(\delta_{\vec{k}})/T_e$ (13) as a function of the wave number and the angle $\delta_{\vec{k}}$ between temperature gradient and the wave vector $\vec{k}$. The turbulence parameter K_N (15) equals 5. The rest of the parameters are as in Fig. 5.

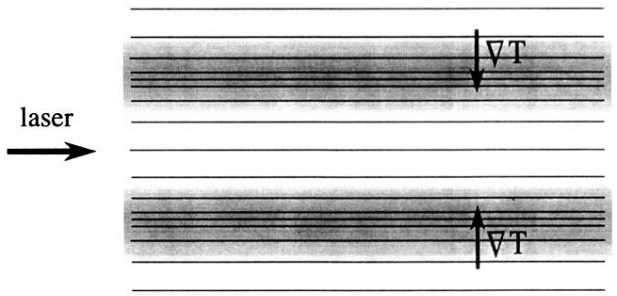

FIG. 8. The schematic diagram of the constant temperature lines based on the results of numerical simulations shown in Fig. 3. Ion acoustic turbulence is excited in the shaded regions around the laser beam axis.